Bulk and interface spin-orbit torques in Pt/Co/MgO thin film structures

M. S. Gabor ,[1,*] M. Belmeguenai,[2] and I. M. Miron[3]

[1]*Center for Superconductivity, Spintronics and Surface Science, Physics and Chemistry Department,*
Technical University of Cluj-Napoca, Str. Memorandumului, 400114 Cluj-Napoca, Romania
[2]*Université Sorbonne Paris Nord, LSPM, CNRS, UPR 3407, F-93430 Villetaneuse, France*
[3]*Université Grenoble Alpes, CNRS, CEA, Grenoble INP, SPINTEC, 38054 Grenoble, France*

We investigate the origin of spin-orbit torques (SOTs) in archetypical Pt/Co/MgO thin films structures by performing harmonic Hall measurements. The behavior of the dampinglike (DL) effective field (h_{DL}) with varying the Pt layer thickness and the Co layer thickness indicates that bulk spin-Hall effect (SHE) in Pt is mainly responsible for DL-SOT. The insertion of a Pd ultrathin layer at the Pt/Co interface leads to a step decrease in h_{DL}, attributed to the modification of interfacial spin transparency. Further increase in Pd thickness leads to a reduction of the interfacial spin-orbit coupling (iSOC) quantified by the decrease in the surface magnetic anisotropy. The consistent insensitivity of h_{DL} to variations in iSOC at the bottom Pt/Co interface and oxidation at the top Co/MgO interface provides additional evidence for the bulk SHE origin of DL-SOT. The strong reduction in the fieldlike (FL) torque effective field (h_{FL}) with decreasing iSOC at the Pt/Co interface points to the interfacial nature of FL-SOT, either due to iSOC-induced interfacial spin currents or to the Rashba-Edelstein effect at the Pt/Co interface. Furthermore, we demonstrate that a FL-SOT develops at the top Co/MgO interface opposing the one generated at the bottom Pt/Co interface, the strength of which increases with Co/MgO interfacial oxidation, and is attributed to the Rashba-Edelstein effect.

I. INTRODUCTION

The current-induced spin-orbit torques (SOTs) in heavy-metal (HM)/ferromagnet (FM) heterostructures [1,2] have garnered remarkable research interest for the development of electrically controlled spintronic and spin-logic devices [3–9]. Two types of mechanisms are generally considered for the microscopic origin of SOTs: either bulk or interface related. In one case, the spin-Hall effect (SHE) [10,11] due to the spin-orbit coupling (SOC) in the bulk of the HM layer produces a spin current propagating towards the HM/FM interface. There, it is partially or totally absorbed by the FM layer as torques on the magnetization. The other mechanism, inverse spin galvanic effect or the Rashba-Edelstein effect (REE), occurring at interfaces with broken-inversion symmetry, involves an in-plane charge current generating a spin accumulation via interface spin-orbit coupling (iSOC), ultimately exerting torques on the magnetization of the FM layer through exchange coupling [12]. Recently, other interfacial mechanisms based on iSOC were proposed to generate SOTs at the HM/FM interfaces [13–15]. Both the bulk and interfacial mechanisms are expected to produce two types of torques on the magnetization with different symmetries: dampinglike (DL) and fieldlike (FL) [11,16–19].

From an applications perspective, it is of major importance to disentangle the origin of SOTs for a particular HM/FM structure to facilitate their optimization. Given that both bulk and interface mechanisms can coexist within the same samples, unraveling the exact nature of the SOTs is not a straightforward experimental task. Varying the thickness of the HM layer to test the SHE as a possible origin for SOTs influences the electrical resistivity of the HM, which, in turn, affects the generation of spin current via the SHE [20]. It could also influence the strains in the HM/FM or even the interfacial morphology, which would impact the SOTs [21]. On the other hand, engineering the interfaces to modify the iSOC might also modify the SOTs beyond the interface-related mechanism. It could strongly affect the current distribution within the stack or it could impact the spin memory loss (SML) at the HM/FM interface and alter the SOTs generated by the bulk SHE [22,23].

In this paper, we investigate the nature of the SOTs in the archetypical Pt/Co/MgO thin films structure. In this type of structure three possible mechanisms could produce both DL and FL SOTs on the FM layer magnetization: (i) SHE in Pt, (ii) REE and/or interfacial spin currents induced by iSOC at the Pt/Co interface, and (iii) REE at the top Co/MgO interface. Initially, we explore the dependence of the DL-SOT and FL-SOT on the Pt layer thickness, revealing that SHE is the main source of DL-SOT [mechanism (i)]. Upon varying the Co layer thickness, DL-SOT behaves as expected for SHE, while FL-SOT deviates from the expected behavior, suggesting the influence of the other interfacial mechanisms beyond the SHE. Furthermore, we engineer the Pt/Co interface by the insertion of an ultrathin Pd layer to tune the iSOC. Interestingly, DL-SOT does not scale with iSOC, while the FL-SOT strongly correlates with it, indicating that the

*mihai.gabor@phys.utcluj.ro

REE-like interfacial mechanism (ii) is dominant for FL-SOT. Last, by adjusting the oxidation level at the Pt/Co interface through changes in the MgO layer thickness we find that DL-SOT remains unaffected, whereas FL-SOT scales with the Co/MgO surface magnetic anisotropy, which is a measure of the interfacial charge transfer affecting the Rashba field at this interface. These findings suggest that REE mechanism (iii) does not impact the DL-SOT, even though it is instrumental in generating the FL-SOT.

II. EXPERIMENT

All the samples studied here were grown at room temperature on thermally oxidized silicon substrates using an ultrahigh-vacuum system that integrates electron-beam evaporation and magnetron sputtering. The typical sample configuration is as follows: Si/SiO$_2$//Ta (2)/Pt (t_{Pt})/Co (t_{Co})/MgO (2)/Ta (1.5), with the values in parentheses indicating the thicknesses in nanometers. Additional samples were also grown, and their structural details will be addressed later in the text. The 2-nm-thick tantalum (Ta) seed layer was deposited using direct current (dc) sputtering onto the substrate under an argon pressure of 1 mTorr. Subsequently, the argon gas was purged from the system, and the remaining structure was deposited through electron-beam evaporation. Throughout the deposition of metallic layers, the chamber pressure remained within the 10^{-10}-Torr range, whereas during the evaporation of MgO, the pressure increased to around 10^{-8} Torr. To protect the structure from contamination due to exposure to the atmosphere, a 1.5-nm-thick Ta capping layer was dc sputtered on the substrate under an argon pressure of 1 mTorr. For the fabrication of the active part of the samples we used the electron-beam evaporation technique due to its ability to generate well-defined interfaces compared to sputtering. Moreover, the directional nature of the incoming atomic flux allowed for the deposition of wedge-shaped layers using a movable shutter placed in front of the substrate. The specificity of the wedge ensured the simultaneous deposition of each series of samples, thereby eliminating material variations that might arise in sequential deposition runs.

The saturation magnetization of the samples was measured at room temperature using a vibrating sample magnetometer. For magnetoelectric experiments, the samples were patterned through conventional UV photolithography and argon-ion milling techniques. A dual-photoresist process was employed to create an undercut in the photoresist mask, reducing edge roughness and redeposition during the milling process. Electrical resistance measurements were performed using the standard four-point technique, while the evaluation of SOTs was carried out using the harmonic Hall voltage technique [24–27].

III. RESULTS AND DISCUSSION

One of the experimental approaches used to investigate the bulk and interfacial characteristics of SOTs involves studying their dependence on the thickness of the heavy-metal Pt layer (t_{Pt}). In principle, effects arising from the REE or other interfacial interactions should remain independent of t_{Pt}, whereas effects due to the bulk SHE would depend on

t_{Pt}, for thicknesses of the order of the spin-diffusion length. Thus, the thickness dependence of the torques should provide information about their physical origin. However, it is important that the overall structure and morphology (crystallinity of the layers, interfacial roughness, interdiffusion processes) remain as much as possible unchanged upon modifying t_{Pt}. This helps to minimize other factors influencing the SOTs. To this end, we deposited a Si/SiO$_2$//Ta (2)/Pt (1.5–5)/Co (2)/MgO (2)/Ta (1.5) sample stack in which the Pt film was grown as a wedge layer over 20 mm. A series of 50×10-µm Hall crosses with increasing t_{Pt} were patterned on the substrate along the wedge direction and diced for magnetoelectric measurements. Figure 1(a) shows a schematic representation of the SOT's harmonic Hall voltage measurement geometry. Since all the samples are in-plane magnetized, we used a variant of the harmonic Hall method adapted for such samples by Avci *et al.* [28], which provides a straightforward method of excluding the thermoelectric effects. The technique involves injecting an alternating current ($I_\omega = I \sin \omega t$) into the patterned stripe (along $\hat{x}$) and measuring the first ($R_\omega = V_\omega/I$) and the second ($R_{2\omega} = V_{2\omega}/I$) harmonic Hall resistances (along $\hat{y}$), while rotating the magnetization in plane by applying an external in-plane rotating magnetic field (H). The R_ω provides information about the planar Hall effect as [28] $R_\omega = R_{PHE} \sin 2\varphi_H$, where R_{PHE} is the planar Hall resistance and φ is the azimuthal angle of the magnetization from the current direction [Fig. 1(b)]. The samples have a relatively weak in-plane uniaxial anisotropy; thus, the magnetization follows the external applied magnetic field and the φ azimuthal angle of the magnetization practically duplicates the φ_H azimuthal angle of the field. The second-harmonic Hall resistance $R_{2\omega}$ contains information about the SOT effective fields and it is given by [28]

$$R_{2\omega} = \frac{1}{2}\left(R_{AHE}\frac{h_{DL}}{H + H_k} + R_{\nabla T}\right)\cos\varphi$$
$$+ R_{PHE}(2\cos^3\varphi_H - \cos\varphi_H)\frac{h_{FL} + h_{Oe}}{H},$$

where, respectively, R_{PHE} and R_{AHE} are the planar and anomalous Hall resistances, h_{DL} and h_{FL} are the dampinglike and fieldlike effective fields, H_k is the perpendicular anisotropy field, $R_{\nabla T}$ is the second-harmonic Hall resistance due to thermoelectric effects, and h_{Oe} is the Oersted field produced by the charge current passing through the HM layer. R_{AHE} and H_k are determined by applying an out-of-plane field and measuring the transverse voltage (V_{xy}) which is then divided by the electrical current (I) passing through the device to give the transverse resistance $R_{xy} = V_{xy}/I$. The R_{AHE} is calculated as $[R_{xy}(+M_z) - R_{xy}(-M_z)]/2$, where $R_{xy}(+/-M_z)$ is the transverse resistance for positive (negative) saturation. The inset of Fig. 1(c) shows a representative AHE resistance measurement where the R_{AHE} and the $\mu_0 H_k$ are indicated. By fitting the $R_{2\omega}$ experimental data to the above equation, two contributions can be extracted: one which shows a $\cos\varphi_H$ dependence and gives information about h_{DL}, and another which shows a $2\cos^3\varphi_H - \cos\varphi_H$ dependence and gives information about h_{FL} [Fig. 1(b)]. The h_{DL} and the $R_{\nabla T}$ are obtained from the slope and the intercept of the linear fit of the $\cos\varphi_H$ contribution dependence on the inverse of the sum of the external and
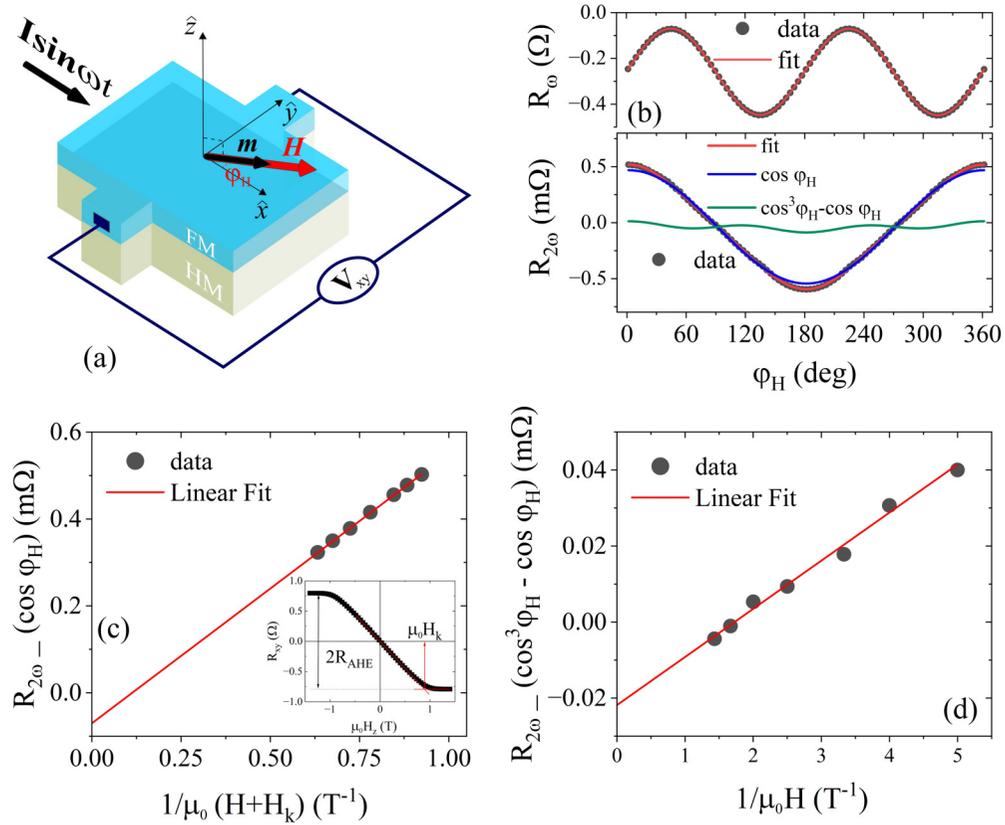
FIG. 1. (a) Schematic representation of the harmonic Hall magnetotransport measurement geometry. (b) First- and second-harmonic Hall resistances, as a function of the azimuthal angle of the external in-plane magnetic field with the current direction, for the Pt (4.68)/Co (2)/MgO (2) representative sample. The points are experimental data while the continuous lines are fits using the equations from the main text. Dependence of the second-harmonic Hall resistance (c) $\cos \varphi_H$ contribution on $1/\mu_0(H + H_k)$ and (d) $2\cos^3\varphi_H - \cos \varphi_H$ contribution on $1/\mu_0 H$, used to extract the h_{DL} and the h_{FL}. The straight lines are linear fits to the data. The inset in (c) shows the transverse resistance as a function of the perpendicular applied field, used to extract R_{AHE} and $\mu_0 H_k$.

anisotropy fields [Fig. 1(c)]. The sum $h_{FL} + h_{Oe}$ is determined from the slope of the linear fit of the $2\cos^3\varphi_H - \cos \varphi_H$ contribution dependence on the inverse external field [Fig. 1(d)]. The Oersted field is calculated as $h_{Oe} = \mu_0 j_{Pt} t_{Pt}/2$, where j_{Pt} is the charge-current density through the Pt layer, and it is subtracted from the $h_{FL} + h_{Oe}$ sum to obtain h_{FL}. The j_{Pt} was calculated by assuming a parallel resistor model and by subtracting the contribution to the total resistance of the Ta (2)/Co (2)/MgO (2)/Ta (1.5) stack, measured on a sample deposited on the same run (see Supplemental Material [29]).

Figure 2 shows the dampinglike (h_{DL}/j_{Pt}, h_{DL}/E) and fieldlike (h_{FL}/j_{Pt}, h_{FL}/E) effective fields normalized by either the charge-current density through the Pt layer or by the applied electric field ($E = \rho_{Pt} j_{Pt}$). Irrespective of the normalization procedure, the effective fields show an increase with increasing t_{Pt}, with a tendency for saturation at larger t_{Pt}. Both the values and the behavior are in agreement with literature [20]. Moreover, this type of effective fields' HM thickness dependence is a recurring feature in various systems that rely on different HM layers [30–34]. Our findings are consistent with first-principles calculations based on the drift-diffusion formalism of the SHE. These calculations suggest that both dampinglike and fieldlike torques should exhibit a similar dependence on the thickness of the heavy-metal layer and that the dampinglike torque should be significantly larger

than the fieldlike torque given their direct proportionality to the real and imaginary parts of the spin-mixing conductance [16]. Thus, our results seem to indicate that the SHE is the main source of the spin current responsible for the two types of torques. Nonetheless, caution should be exercised in drawing a conclusive statement. REE-like interfacial mechanisms generating the torques might be dominated by the SHE for relatively large HM thicknesses. Therefore, even smaller thicknesses of the HM layer should be probed to evidence interfacial effects [16,17]. However, further reducing the thickness of the HM layer may bring additional complications. The resistivity of the Pt layer increases strongly with decreasing thickness [29], which affects the spin-current generation via SHE [20] and also the charge-current distribution within the stack. Also, first-principles calculations showed that the strains, which are expected to increase with decreasing the HM thickness, have a strong impact on both dampinglike and fieldlike torques [35]. Moreover, reducing the thickness could influence the HM/FM interfacial morphology affecting the spin-current transmission across the interface or interfacial spin-current generation.

Further, one can examine the torques' dependence on the thickness of the ferromagnetic layer (t_{Co}). If the bulk SHE within the Pt layer is the source of the torques, and as a result, the source of the torques lies outside the Co layer, one would
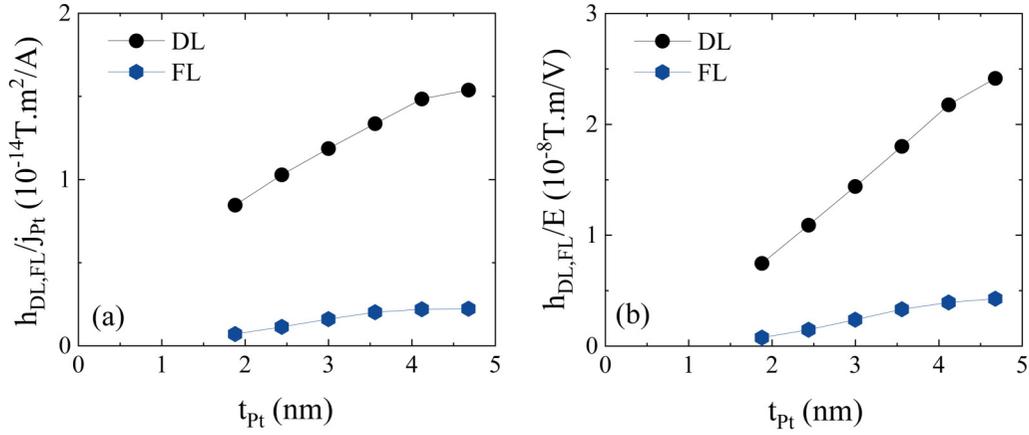
FIG. 2. Dampinglike (h_{DL}) and fieldlike (h_{FL}) effective fields normalized by the (a) charge-current density through the Pt layer (j_{Pt}) and by (b) the applied electric field ($E = \rho_{Pt} j_{Pt}$), as a function of the Pt layer thickness (t_{Pt}).

expect the effective fields to be inversely proportional to the thickness of the Co layer ($\propto 1/t_{Co}$) [16]. To study this, we fabricated a series of samples with the structure Si/SiO$_2$//Ta (2)/Pt (5)/Co (1.4–4)/MgO (2)/Ta (1.5), maintaining a constant Pt layer thickness while varying the Co layer thickness in a wedgelike manner. Figure 3 shows the h_{DL}/j_{Pt} and h_{FL}/j_{Pt} as a function of the inverse Co layer thickness ($1/t_{Co}$). From Fig. 3(a) one can observe that h_{DL}/j_{Pt} decreases linearly with $1/t_{Co}$, indicating that the bulk SHE is the main source of h_{DL}. As seen in Fig. 3(b), h_{FL}/j_{Pt} deviates from the linearity and does not corelate with h_{DL}/j_{Pt}. This suggests the presence of an additional interfacial mechanisms contributing to the h_{FL}. It is to be mentioned that a deviation from the perfect $1/t_{Co}$ dependence is expected as long as the *interfacial layers* where spin-current generation or spin accumulation take places have a finite thickness [12,36–38]. A similar behavior is expected for the SHE-induced h_{FL} when the thickness of the ferromagnetic layer is below the spin decoherence length [39]. However, this does not apply to our samples because the thickness of the Co layer exceeds the spin decoherence length for Co, which is approximately 1.2 nm [40]. We can also rule out the effect of strains in the Co layer, at least for thicknesses larger than 1.5 nm. Magnetic anisotropy measurements [29],

which are highly sensitive to strains in Co [41], did not indicate the presence of significant strains.

Interface effects influencing the SOTs could be associated with either the Pt/Co or Co/MgO interfaces, or possibly both. First, we will consider the bottom Pt/Co interface. REE or other interfacial-related mechanisms generating torques rely on the interfacial spin-orbit coupling [13,16]; thus, tuning the iSOC could provide insight into the interfacial generation of the SOTs. Our strategy to tune the iSOC is to insert an ultrathin Pd layer at the interface between Pt and Co. Hence, we fabricated a series of samples with the structure Si/SiO$_2$//Ta (2)/Pt (5)/Pd (0–1.8)/Co (2)/MgO (2)/Ta (1.5), maintaining Pt- and Co-layers' thicknesses constant, while varying the Pd layer thickness in a wedgelike manner. We selected Pd as an interlayer for several reasons. Pt and Pd share similar crystal structures, both belonging to the Fm-$3m$ space group, with closely matched lattice parameters ($a_{Pt} = 0.392$ nm and $a_{Pd} = 0.389$ nm), which facilitates the high-quality layer-by-layer growth of Pd on Pt. They also exhibit comparable bulk electrical resistivities ($\rho_{Pt} = 106$ nΩm and $\rho_{Pd} = 105$ nΩm), ensuring a uniform current flow in the Pt/Pd bilayer [29]. Moreover, Pd has a lower SOC than Pt and a relatively large spin-diffusion length ($\lambda_{sd} \sim 8$ nm) [21].
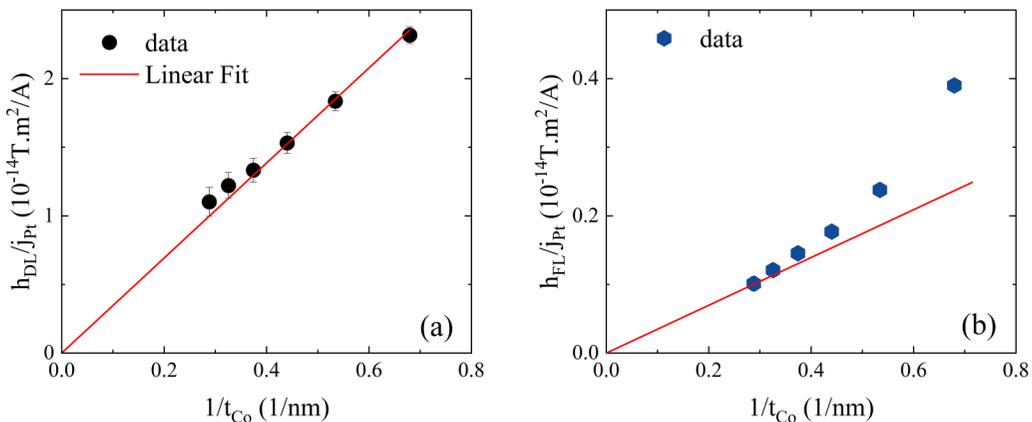
FIG. 3. (a) Dampinglike (h_{DL}/j_{Pt}) and (b) fieldlike (h_{FL}/j_{Pt}) effective fields normalized by the charge-current density through the Pt layer (j_{Pt}) as a function of the inverse Co layer thickness ($1/t_{Co}$). The line in (a) is a linear fit, while in (b) the line is drawn from the origin through the first data point.
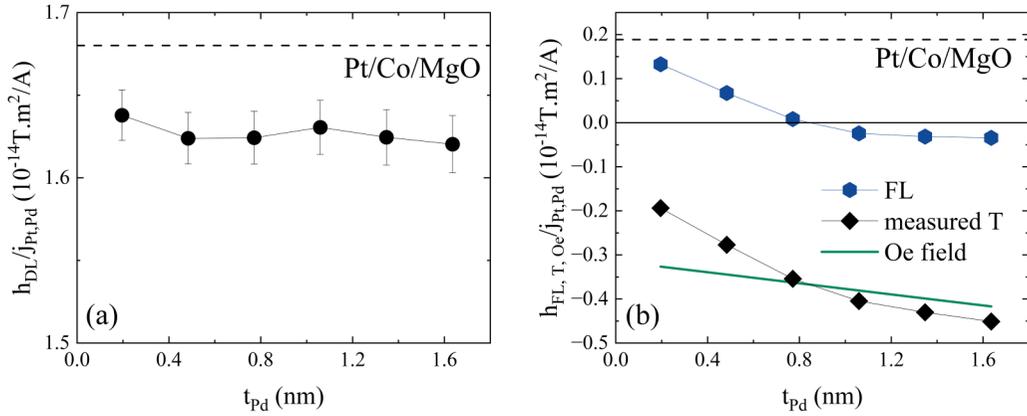
FIG. 4. (a) Dampinglike ($h_{DL}/j_{Pt,Pd}$) and (b) fieldlike ($h_{FL}/j_{Pt,Pd}$) effective fields normalized by the charge-current density through the Pt/Pd bilayer ($j_{Pt,Pd}$) as a function of the thickness of the Pd layer. The measured transverse effective field (measured T) and the Oersted field, extracted from the measured transverse effective field to determine the h_{FL}, are also displayed. The dashed lines indicate the corresponding effective field values for the samples without the interfacial Pd layer.

Figure 4(a) shows the dampinglike ($h_{DL}/j_{Pt,Pd}$) effective field normalized by the charge-current density through the Pt/Pd bilayer ($j_{Pt,Pd}$) as a function of the thickness of the Pd layer (t_{Pd}). The $h_{DL}/j_{Pt,Pd}$ does not show a clear dependence on t_{Pd}; it remains constant within the error bars for the entire t_{Pd} range. It is noteworthy to observe that that the insertion of the Pd layer leads to a decrease around 5% in $h_{DL}/j_{Pt,Pd}$ compared to the Pt/Co/MgO sample without the Pd insertion layer. The fieldlike effective field ($h_{FL}/j_{Pt,Pd}$) normalized by $j_{Pt,Pd}$ is shown in Fig. 4(b) and displays a different behavior. It exhibits a continuous decrease with t_{Pd} up to approximately a 1-nm thickness, after which it remains relatively constant. It is also interesting to observe that $h_{FL}/j_{Pt,Pd}$ changes sign for t_{Pd} larger than approximately 0.8 nm. For clarity, in Fig. 4(b) the measured transverse effective field and the Oe field, extracted from the measured transverse effective field to determine the h_{FL}, are also displayed.

We recently showed that the insertion of an ultrathin Pd layer at the Pt/Co interface can effectively screen the SOC of Pt [42]. Moreover, it is well known that the surface magnetic anisotropy (K_s) at the HM/Co interface is related to the iSOC-enhanced interface orbital magnetic moments [43]. Hence, the variation of iSOC with respect to t_{Pd} could be assessed by

measuring the dependence of K_s on t_{Pd} [29]. Figure 5 shows the $h_{DL}/j_{Pt,Pd}$ and $h_{FL}/j_{Pt,Pd}$ as a function of K_s. Interestingly, $h_{DL}/j_{Pt,Pd}$ does not scale with K_s, while $h_{FL}/j_{Pt,Pd}$ shows a linear correlation with K_s.

We will start by examining the behavior of $h_{DL}/j_{Pt,Pd}$. The reduction of $h_{DL}/j_{Pt,Pd}$ with the insertion of the Pd layer relative to the Pt/Co/MgO sample can be understood by considering the various mechanisms involving SHE and interface-generated spin currents, or a combination of both. This decrease could be attributed to the SML at the interface [22,44], which reduces the SHE-generated spin-current transmission through the interface [45]. However, this effect is unlikely as it involves the loss of spin information due to spin-flip scattering, which should increase with iSOC [23] and, therefore, with K_s. This is contrary to our observation that the decrease is independent of K_s [Fig. 5(a)]. Another possibility is that the Pd layer produces a spin current via SHE opposing the one produced by the Pt layer. This is also not likely having in view the large spin-diffusion length of Pd relative to t_{Pd} and the relatively low spin-Hall angle of Pd [21,34]. Another possibility is the generation of spin currents at the Pd/Co interface producing a h_{DL} opposing the one produced via the bulk SHE in Pt. Theoretical calculations indicated that
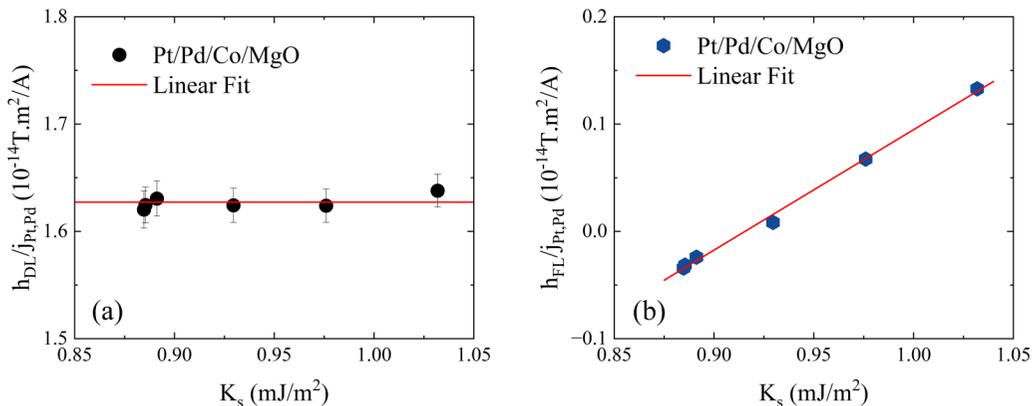
FIG. 5. (a) Dampinglike ($h_{DL}/j_{Pt,Pd}$) and (b) fieldlike ($h_{FL}/j_{Pt,Pd}$) effective fields normalized by the charge-current density through the Pt-Pd layer ($j_{Pt,Pd}$) as a function of the surface magnetic anisotropy (K_s). The lines are linear fits to the data.

spin currents could be generated by interfaces when iSOC is present [17,46], or even at the interface between a low SOC normal metal and ferromagnetic material [13]. Although we cannot exclude this possibility, it is not likely to be the case since one would expect a variation of h_{DL} with iSOC, and thus K_s. Another plausible mechanism, consistent with our observations and independent of iSOC, is the modification of the spin transparency at the Pt/Co interface by introducing the Pd layer. This is an electronic effect concerning the transmission and reflection of electrons carrying angular momentum. It is linked to the electronic band matching of the two metals across the interface and is not associated with the loss of spin polarization [47].

The behavior of $h_{FL}/j_{Pt,Pd}$ is quite different. Besides the similar initial reduction with the insertion of the thinnest Pd layer, $h_{FL}/j_{Pt,Pd}$ scales linearly with K_s and, thus, with iSOC. This indicates that besides SHE there is another interfacial mechanism responsible for h_{FL}. The reduction of h_{FL} by the insertion of the Pd layer [Fig. 4(b)] and the linear correlation K_s [Fig. 5(b)] indicates that the primary mechanism responsible for generating h_{FL} is of an interfacial nature. This could be attributed to either REE-like mechanism [16,37,48] or interfacial spin currents induced by iSOC [13,17], which result in a net interfacial spin accumulation responsible for h_{FL}. One might argue that the insertion of the Pd layer diminishes the proximity-induced magnetization (PIM) in Pt, providing a potential mechanism for altering h_{FL} through the dephasing of the spin accumulation by the PIM exchange field, as an alternative to the variation of the iSOC. However, it was shown that PIM in Pd/Co is only marginally lower than in Pt/Co [49]. Furthermore, the decrease of the PIM is expected to increase h_{FL} and not diminish it [50].

As we will demonstrate in the following sections, the observed sign change of $h_{FL}/j_{Pt,Pd}$ for t_{Pd} larger than about 0.8 nm can be attributed to the emergence of a FL-SOT at the top Co/MgO interface, which possesses an opposite sign compared to the one at the bottom Pt/Co interface. The reason $h_{FL}/j_{Pt,Pd}$ remains constant with further increase of t_{Pd} is because roughly 1 nm of Pd is sufficient to screen the SOC of Pt [42]. Further increasing the Pd layer thickness will not further reduce the iSOC. It will remain constant and associated with the iSOC of the Pd/Co interface, which, although smaller than the one related to the Pt/Co interface, is not negligible.

To summarize, our data indicate that h_{DL} is primarily generated via the bulk SHE from Pt, and the decrease in h_{DL} following the insertion of the Pd layer can be attributed to the variation of the interfacial spin transparency. At the same time, besides SHE, the results suggests that the primary mechanism responsible for h_{FL} is of interfacial nature related either to iSOC-induced interfacial spin currents or to REE at the Pt/Co interface. Since the current flow through the Pt/Pd bilayer is uniform [29], the linear relationship between h_{FL} and K_s will hold, even when h_{FL} is normalized by the charge-current density through the Pd interlayer (h_{FL}/j_{Pd}). This supports our observation that the primary mechanism responsible for h_{FL} is of interfacial nature.

Up to this point, we focused on examining the impact of the bottom Pt/Co interface on the SOTs. However, it is also reasonable to consider that the top Co/MgO interface may play a significant role in SOT generation. For this purpose,

we deposited a series of Si/SiO$_2$//Ta (2)/Pt (5)/Co (2)/MgO (0–3.6)/Pt (5) samples, where the MgO was grown as a wedge layer with thicknesses ranging up to 3.6 nm. The Ta (1.5) capping layer was replaced with a Pt (5) film for two main reasons. It will allow us to study the impact on SOTs upon continuously separating the Co/Pt interface. Also, when the MgO layer is sufficiently thick, the top Pt layer is expected to generate only an Oersted field countering the one produced by the bottom Pt layer, thus making the determination of h_{FL} more reliable [29].

Figure 6(a) shows the electrical resistance (R_{xx}) of the stacks as a function of the MgO layer thickness (t_{MgO}). Initially, there is a relatively strong increase in R_{xx} with t_{MgO}. This increase is most likely attributed to the discontinuity of the MgO layer within this thickness range, which increases interface scatterings and subsequently leads to a higher R_{xx}. As t_{MgO} increases, the layer becomes continuous and R_{xx} starts to drop. Interestingly, above a MgO layer thickness corresponding to 3–4 atomic planes, the R_{xx} falls below that of the sample with no MgO layer. In the case of the Pt/Co/Pt sample, it is probable that there is some degree of intermixing at the Co/Pt interface, leading to increased interface scatterings. The introduction of the MgO layer serves to prevent this intermixing, resulting in a decrease in R_{xx}. However, for larger MgO thicknesses, the R_{xx} exhibits a slight increase of approximately 2%, which we attribute to a minor oxidation of the Co layer with increasing MgO layer thickness. This small variation of R_{xx} for t_{MgO} above 0.6–0.7 nm ensures that the current distribution remains relatively unchanged upon increasing t_{MgO} up to 3.6 nm. The behavior of the R_{AHE} as a function of t_{MgO}, shown in the inset of Fig. 6(a), is consistent with that of R_{xx}. It initially decreases, after which it remains relatively independent of t_{MgO}. With the insertion of the MgO layer, the Co/Pt interface contribution to AHE is eliminated, resulting in the initial decrease of R_{AHE} with t_{MgO}.

Figure 6(b) shows the saturation magnetization (M_s) and the surface magnetic anisotropy (K_s) as a function of t_{MgO}. The M_s shows a slight linear decrease with increasing t_{MgO}. This implies a soft oxidation of the Co layer as more oxygen becomes available for larger t_{MgO}. It corresponds to an oxidation of about 0.11 nm of Co for the largest t_{MgO}. This is also reflected in the evolution of the surface magnetic anisotropy, which shows a strong decrease with the thickness of the MgO layer. It is well known that the surface magnetic anisotropy at the Co/MgO interface is related to the hybridization between O p and Co d_{z^2} orbitals, and that it decreases strongly in the case of suboptimal (over- or under) oxidation of the Co layer [51–53].

Figure 7(a) shows the h_{DL}/j_{Pt} and h_{FL}/j_{Pt} as a function of t_{MgO}. The two effective fields h_{DL} and h_{FL} were normalized by the charge-current density through the bottom Pt layer and were corrected by a factor that accounts for the slight decrease in M_s with t_{MgO}, considering that the effective fields should scale inversely with the magnetic volume. Concerning h_{DL}, it starts from a negligibly small value, shows an abrupt increase, and then remains relatively constant as a function of t_{MgO}. This behavior can be understood by considering SHE in Pt as the main source of h_{DL}. In the case of the symmetric Pt/Co/Pt structure, the effects of SHE generated by the spin currents from the top and bottom Pt layers cancel each other out,
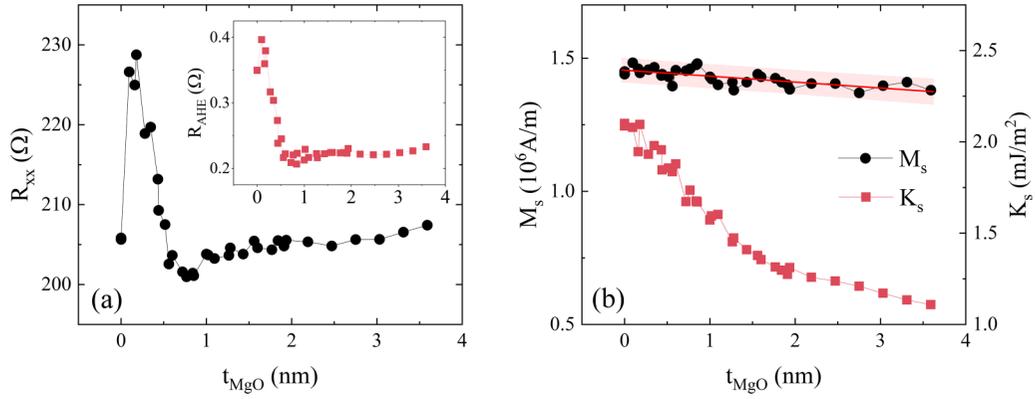
FIG. 6. (a) Longitudinal electrical resistance (R_{xx}), the anomalous Hall resistance (R_{AHE}), (b) saturation magnetization (M_s), and surface magnetic anisotropy (K_s) as a function of the MgO layer thickness (t_{MgO}). The straight line is a linear fit of the M_s vs t_{MgO}.

rendering h_{DL} negligibly small. However, as t_{MgO} is increased and the MgO layer becomes continuous, the spin current from the top Pt layer is blocked, and h_{DL} is determined solely by the spin current from the bottom Pt layer, which does not depend on the MgO layer thickness. Thus, h_{DL} remains independent of t_{MgO} for values larger that 0.6–0.7 nm.

The behavior of h_{FL} is quite different. Unlike h_{DL}, in the case of the symmetric Pt/Co/Pt structure, the h_{FL} is not negligibly small. Moreover, after the first increase, h_{FL} decreases with t_{MgO}, rather than remaining constant as h_{DL}. This indicates the existence of an additional mechanism at the Co/MgO interface influencing the FL-SOT.

The reduction of PIM in the top Pt layer with increasing t_{MgO} could, in principle, affect h_{FL}. Nonetheless, even if this is the case, for the MgO layer thicknesses larger than 0.6–0.7 nm, for which the MgO layer is continuous, one would expect the PIM in Pt to become negligible, since ultrathin interlayers are known to extinguish the PIM at the Pt/Co interface [49]. Because h_{FL} is decreasing even above this thickness, the observed reduction cannot be attributed to a decrease of PIM.

Oxygen migration towards the bottom Pt/Co interface could also affect the FL-SOT. To exclude this possibility, we performed additional measurements of the interfacial Dzyaloshinskii-Moriya interaction (iDMI) using Brillouin light-scattering spectroscopy [29]. iDMI is an interfacial interaction which is mainly given by the Pt/Co interface in Pt/Co/MgO structures [54]. In case of oxygen migration towards the bottom Pt/Co, one would expect the DMI to be affected since the interaction is extremely sensitive to interfacial details [42]. Figure 7(a) shows the effective iDMI constant (D_{eff}) alongside h_{DL}/j_{Pt}, as a function of t_{MgO}. Except for the symmetric Pt/Co/Pt structure with $t_{MgO} = 0$, the D_{eff} and h_{DL}/j_{Pt} follow the same trend and remain independent of t_{MgO} for thicknesses larger than 0.7 nm. This indicates that for t_{MgO} up to 0.7 nm the iDMI at the bottom Pt/Co interface and top Co/MgO/Pt interface adds destructively and the iDMI at the top Co/MgO/Pt interface decreases with increasing t_{MgO}. Furthermore, since for t_{MgO} larger than 0.7 nm the D_{eff} value is in agreement with the one expected for the Pt/Co interface [42,55], it follows that the iDMI at the top Co/MgO/Pt interface becomes negligibly small and the iDMI at the bottom Pt/Co interface is unaffected by increasing the MgO layer thickness.

Interestingly, for the symmetric Pt/Co/Pt structure both D_{eff} and h_{FL}/j_{Pt} have non-negligible values. This can be understood by considering that both iDMI and FL-SOT are of interfacial nature and scale with iSOC. The bottom Pt/Co surface anisotropy was estimated to be $K_s^{Pt/Co} = 1.26 \pm 0.05$ mJ/m^2 (see Fig. S4 from Ref. [29]) by considering that only this interface contributes to K_s. At the same time, the surface anisotropy for the symmetric Pt/Co/Pt structure is $K_s^{Pt/Co/Pt} = 2.1 \pm 0.05$ mJ/m^2 [see Fig. 6(b)]. This shows that the top Co/Pt interface contributes a maximum of
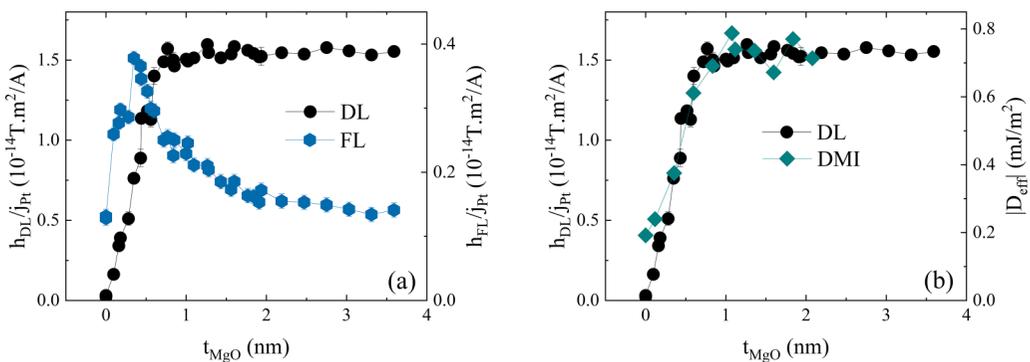
FIG. 7. (a) Dampinglike ($h_{DL}/j_{Pt,Pd}$) and fieldlike (h_{FL}/j_{Pt}) effective fields normalized by the charge-current density through the Pt layer (j_{Pt}) as a function of the MgO layer thickness (t_{MgO}). (b) The effective iDMI constant and h_{DL}/j_{Pt}, as a function of t_{MgO}.
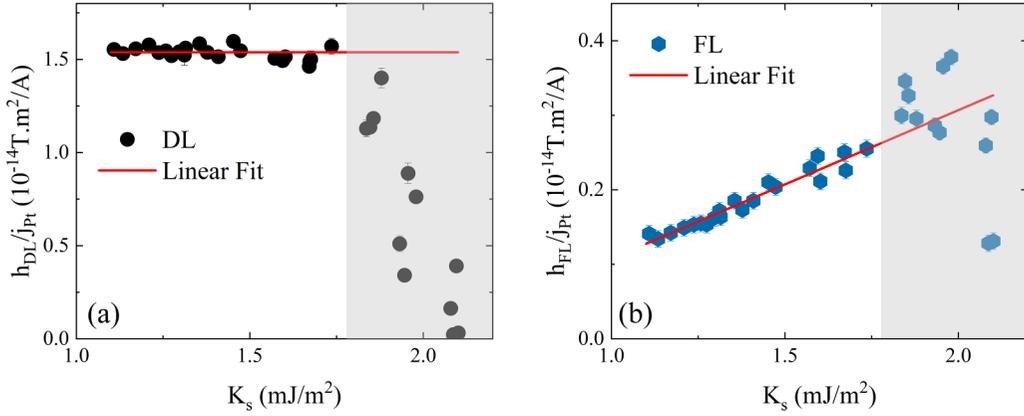
FIG. 8. (a) Dampinglike (h_{DL}/j_{Pt}) and (b) fieldlike (h_{FL}/j_{Pt}) effective fields normalized by the charge-current density through the Pt layer (j_{Pt}) as a function of surface magnetic anisotropy (K_s). The shaded areas correspond to MgO layer thickness lower than 0.72 nm. The lines are linear fits of the points outside the shaded areas.

$K_s^{Co/Pt} = 0.84 \pm 0.1$ mJ/m^2 to the total surface magnetic anisotropy. The presence of larger interfacial anisotropy arising from the bottom Pt/Co interface than from the top Co/Pt one is a known feature in Pt/Co/Pt structures [56,57]. Given that the surface magnetic anisotropy at the Pt/Co and Co/Pt interfaces scales with iSOC, it can be inferred that the iSOC at the bottom Pt/Co interface is higher than at the top Co/Pt interface. Consequently, one expects both iDMI and FL-SOT to be higher at the bottom Pt/Co interface than at the top Co/Pt interface. Therefore, although for the symmetric structure both iDMI and FL-SOT add destructively, they do not cancel out since they have different magnitudes at the two interfaces.

Our experimental observations indicate that the decrease of h_{FL} for t_{MgO} larger than 0.7 nm is not related to the bottom Pt/Co interface, but to the upper Co/MgO one. From Fig. 8(a) one can see that h_{DL}/j_{Pt} does not scale with K_s, which is expected considering that SHE in the bottom Pt layer is responsible for DL-SOT. However, from Fig. 8(b) one can observe that h_{FL}/j_{Pt} and K_s are well corelated, indicating that the same mechanism of interfacial oxidation affects both quantities. First-principles calculations [53] show that the presence of oxygen at the Co surface in Pt/Co structures leads to a transfer of electrons from Co to oxygen and, consequently, to a reduction of K_s, in line with our observations. The decrease of M_s and K_s with increasing t_{MgO} points to the increased Co oxidation and, consequently, to Co to oxygen charge transfer, as more oxygen becomes available with increased t_{MgO}. The Co/MgO interfacial charge transfer also affects the Rashba field at this interface. This, in turn, will affect the FL-SOT generated at the same interface, since they are strongly corelated [16,48,58]. Our results clearly indicate that for $t_{MgO} > 0.7$ nm a FL-SOT develops at the top Co/MgO interface via REE, whose strength increases with t_{MgO} and has a sign opposite the one generated by the SHE or interfacial effects at bottom Pt/Co interface. We would also like to point out that for $t_{MgO} > 0.7$ nm, the R_{xx} exhibits only a slight increase of approximately 2%. This small variation ensures that the current distribution through the stack remains relatively unchanged upon increasing t_{MgO} from 0.6–0.7 nm up to 3.6 nm. Thus, the variations of h_{FL} shown in Figs. 7

and 8, will still hold even if we normalize the h_{FL} by the current density through the Co layer. This furthermore supports our observation that the mechanism responsible for h_{FL} at the Co/MgO interface is the REE.

IV. CONCLUSIONS

In summary, we showed that in the case of the Pt/Co/MgO structures both bulk and interface effects influence the SOTs. We identified three mechanisms responsible for the SOTs acting on the FM layer magnetization: (i) SHE in Pt, (ii) REE and/or interfacial spin currents induced by iSOC at the Pt/Co interface, and (iii) REE at the top Co/MgO interface. The behavior of h_{DL} with varying t_{Pt} and t_{Co} indicates that bulk SHE in Pt is mainly responsible for DL-SOT. The insertion of a Pd ultrathin layer at the Pt/Co interface leads to a decrease in h_{DL}, attributed to the variation of interfacial spin transparency. Additionally, the consistent insensitivity of h_{DL} to variations in iSOC at the bottom Pt/Co interface and oxidation at the Co/MgO interface provides further support for the bulk SHE [mechanism (i)] as the primary source of DL-SOT. Conversely, the behavior of h_{FL} with varying t_{Co} indicates that besides SHE other interfacial mechanisms contribute to FL-SOT. The significant decrease of h_{FL} with decreasing iSOC at the Pt/Co interface points to the dominant interfacial nature of FL-SOT, driven by iSOC-induced interfacial-generated spin currents or REE at the Pt/Co interface [mechanism (ii)]. Moreover, we show that an additional FL-SOT develops at the top Co/MgO interface with opposite sign to the one generated by the SHE or interfacial effects at bottom Pt/Co interface and whose strength increases with Co/MgO interfacial oxidation [mechanism (iii)]. Our experimental results elucidate the origins of SOTs in Pt/Co/MgO structures, resolving ongoing debates about their bulk versus interfacial origins.

---

[1] I. M. Miron, K. Garello, G. Gaudin, P.-J. Zermatten, M. V. Costache, S. Auffret, S. Bandiera, B. Rodmacq, A. Schuhl, and P. Gambardella, Perpendicular switching of a single ferromagnetic layer induced by in-plane current injection, Nature (London) **476**, 189 (2011).

[2] L. Liu, C.-F. Pai, Y. Li, H. W. Tseng, D. C. Ralph, and R. A. Buhrman, Spin-torque switching with the giant spin Hall effect of tantalum, Science **336**, 555 (2012).

[3] S. Fukami, T. Anekawa, C. Zhang, and H. Ohno, A spin–orbit torque switching scheme with collinear magnetic easy axis and current configuration, Nat. Nanotechnol. **11**, 621 (2016).

[4] S. Fukami, C. Zhang, S. DuttaGupta, A. Kurenkov, and H. Ohno, Magnetization switching by spin–orbit torque in an antiferromagnet–ferromagnet bilayer system, Nat. Mater. **15**, 535 (2016).

[5] E. Grimaldi, V. Krizakova, G. Sala, F. Yasin, S. Couet, G. Sankar Kar, K. Garello, and P. Gambardella, Single-shot dynamics of spin–orbit torque and spin transfer torque switching in three-terminal magnetic tunnel junctions, Nat. Nanotechnol. **15**, 111 (2020).

[6] P. P. J. Haazen, E. Murè, J. H. Franken, R. Lavrijsen, H. J. M. Swagten, and B. Koopmans, Domain wall depinning governed by the spin Hall effect, Nat. Mater. **12**, 299 (2013).

[7] G. Yu, P. Upadhyaya, X. Li, W. Li, S. K. Kim, Y. Fan, K. L. Wong, Y. Tserkovnyak, P. K. Amiri, and K. L. Wang, Room-temperature creation and spin–orbit torque manipulation of skyrmions in thin films with engineered asymmetry, Nano Lett. **16**, 1981 (2016).

[8] W. Jiang, X. Zhang, G. Yu, W. Zhang, X. Wang, M. Benjamin Jungfleisch, J. E. Pearson, X. Cheng, O. Heinonen, K. L. Wang, Y. Zhou, A. Hoffmann, and S. G. E. te Velthuis, Direct observation of the skyrmion Hall effect, Nat. Phys. **13**, 162 (2017).

[9] Z. Luo, A. Hrabec, T. P. Dao, G. Sala, S. Finizio, J. Feng, S. Mayr, J. Raabe, P. Gambardella, and L. J. Heyderman, Current-driven magnetic domain-wall logic, Nature (London) **579**, 214 (2020).

[10] J. E. Hirsch, Spin Hall effect, Phys. Rev. Lett. **83**, 1834 (1999).

[11] J. Sinova, S. O. Valenzuela, J. Wunderlich, C. H. Back, and T. Jungwirth, Spin hall effects, Rev. Mod. Phys. **87**, 1213 (2015).

[12] A. Manchon, J. Železný, I. M Miron, T. Jungwirth, J. Sinova, A. Thiaville, K. Garello, and P. Gambardella, Current-induced spin-orbit torques in ferromagnetic and antiferromagnetic systems, Rev. Mod. Phys. **91**, 035004 (2019).

[13] V. P. Amin, J. Zemen, and M. D. Stiles, Interface-generated spin currents, Phys. Rev. Lett. **121**, 136805 (2018).

[14] L. Wang, R. J. H. Wesselink, Y. Liu, Z. Yuan, K. Xia, and P. J. Kelly, Giant room temperature interface spin Hall and inverse spin Hall effects, Phys. Rev. Lett. **116**, 196602 (2016).

[15] K.-W. Kim, K.-J. Lee, J. Sinova, H.-W. Lee, and M. D. Stiles, Spin-orbit torques from interfacial spin-orbit coupling for various interfaces, Phys. Rev. B **96**, 104438 (2017).

[16] P. M. Haney, H.-W. Lee, K.-J. Lee, A. Manchon, and M. D. Stiles, Current induced torques and interfacial spin-orbit coupling: Semiclassical modeling, Phys. Rev. B **87**, 174411 (2013).

[17] V. P. Amin and M. D. Stiles, Spin transport at interfaces with spin-orbit coupling: Phenomenology, Phys. Rev. B **94**, 104420 (2016).

[18] A. Manchon and S. Zhang, Theory of nonequilibrium intrinsic spin torque in a single nanomagnet, Phys. Rev. B **78**, 212405 (2008).

[19] H. Kurebayashi, J. Sinova, D. Fang, A. C. Irvine, T. D. Skinner, J. Wunderlich, V. Novák, R. P. Campion, B. L. Gallagher, E. K. Vehstedt, L. P. Zârbo, K. Výborný, A. J. Ferguson, and T. Jungwirth, An antidamping spin–orbit torque originating from the Berry curvature, Nat. Nanotechnol. **9**, 211 (2014).

[20] M.-H. Nguyen, D. C. Ralph, and R. A. Buhrman, Spin torque study of the spin Hall conductivity and spin diffusion length in platinum thin films with varying resistivity, Phys. Rev. Lett. **116**, 126601 (2016).

[21] X. Tao, Q. Liu, B. Miao, R. Yu, Z. Feng, L. Sun, B. You, J. Du, K. Chen, S. Zhang, L. Zhang, Z. Yuan, D. Wu, and H. Ding, Self-consistent determination of spin Hall angle and spin diffusion length in Pt and Pd: The role of the interface spin loss, Sci. Adv. **4**, eaat1670 (2018).

[22] J. C. Rojas-Sánchez, N. Reyren, P. Laczkowski, W. Savero, J. P. Attané, C. Deranlot, M. Jamet, J. M. George, L. Vila, and H. Jaffrès, Spin pumping and inverse spin Hall effect in platinum: the essential role of spin-memory loss at metallic interfaces, Phys. Rev. Lett. **112**, 106602 (2014).

[23] L. Zhu, D. C. Ralph, and R. A. Buhrman, Effective spin-mixing conductance of heavy-metal–ferromagnet interfaces, Phys. Rev. Lett. **123**, 057203 (2019).

[24] K. Garello, I. M. Miron, C. O. Avci, F. Freimuth, Y. Mokrousov, S. Blügel, S. Auffret, O. Boulle, G. Gaudin, and P. Gambardella, Symmetry and magnitude of spin–orbit torques in ferromagnetic heterostructures, Nat. Nanotechnol. **8**, 587 (2013).

[25] U. H. Pi, K. W. Kim, J. Y. Bae, S. C. Lee, Y. J. Cho, K. S. Kim, and S. Seo, Tilting of the spin orientation induced by Rashba effect in ferromagnetic metal layer, Appl. Phys. Lett. **97**, 162507 (2010).

[26] M. Hayashi, J. Kim, M. Yamanouchi, and H. Ohno, Quantitative characterization of the spin-orbit torque using harmonic Hall voltage measurements, Phys. Rev. B **89**, 144425 (2014).

[27] I. M. Miron, P. J. Zermatten, G. Gaudin, S. Auffret, B. Rodmacq, and A. Schuhl, Domain wall spin torquemeter, Phys. Rev. Lett. **102**, 137202 (2009).

[28] C. O. Avci, K. Garello, M. Gabureac, A. Ghosh, A. Fuhrer, S. F. Alvarado, and P. Gambardella, Interplay of spin-orbit torque and thermoelectric effects in ferromagnet/normal-metal bilayers, Phys. Rev. B **90**, 224427 (2014).

[29] See Supplemental Material at http://link.aps.org/supplemental/10.1103/PhysRevB.109.104407 for more details on the electrical resistance, anomalous Hall resistance, planar Hall resistance, saturation magnetization, and surface magnetic anisotropy of the stacks; and estimation of the Oersted field and details about the Brillouin light-scattering determination of the effective Dzyaloshinskii-Moriya constant, where Refs. [59–64] are also included.

[30] J. Torrejon, J. Kim, J. Sinha, S. Mitani, M. Hayashi, M. Yamanouchi, and H. Ohno, Interface control of the magnetic chirality in CoFeB/MgO heterostructures with heavy-metal underlayers, Nat. Commun. **5**, 4655 (2014).

[31] Q. Hao and G. Xiao, Giant spin Hall effect and switching induced by spin-transfer torque in a W/$Co_{40}Fe_{40}B_{20}$/MgO structure with perpendicular magnetic anisotropy, Phys. Rev. Appl. **3**, 034009 (2015).

[32] M. S. Gabor, T. Petrisor, M. Nasui, M. A. Nsibi, J. Nath, and I. M. Miron, Spin-orbit torques and magnetization switching in perpendicularly magnetized epitaxial Pd/Co_2FeAl/MgO structures, Phys. Rev. Appl. **13**, 054039 (2020).

[33] M. S. Gabor, T. Petrisor, R. B. Mos, A. Mesaros, M. Nasui, M. Belmeguenai, F. Zighem, and C. Tiusan, Spin–orbit torques and magnetization switching in W/Co_2FeAl/MgO structures, J. Phys. D: Appl. Phys. **49**, 365003 (2016).

[34] A. Ghosh, K. Garello, C. Onur Avci, M. Gabureac, and P. Gambardella, Interface-enhanced spin-orbit torques and current-induced magnetization switching of Pd/Co/AlO_x layers, Phys. Rev. Appl. **7**, 014004 (2017).

[35] F. Mahfouzi and N. Kioussis, First-principles study of the angular dependence of the spin-orbit torque in Pt/Co and Pd/Co bilayers, Phys. Rev. B **97**, 224426 (2018).

[36] Y. Du, S. Takahashi, and J. Nitta, Spin current related magnetoresistance in epitaxial Pt/Co bilayers in the presence of spin Hall effect and Rashba-Edelstein effect, Phys. Rev. B **103**, 094419 (2021).

[37] L. Chen, K. Zollner, S. Parzefall, J. Schmitt, M. Kronseder, J. Fabian, D. Weiss, and C. H. Back, Connections between spin-orbit torques and unidirectional magnetoresistance in ferromagnetic-metal–heavy-metal heterostructures, Phys. Rev. B **105**, L020406 (2022).

[38] H. Yang, O. Boulle, V. Cros, A. Fert, and M. Chshiev, Controlling Dzyaloshinskii-Moriya interaction via chirality dependent atomic-layer stacking, insulator capping and electric field, Sci. Rep. **8**, 12356 (2018).

[39] Y. Ou, C.-F. Pai, S. Shi, D. C. Ralph, and R. A. Buhrman, Origin of fieldlike spin-orbit torques in heavy metal/ferromagnet/oxide thin film heterostructures, Phys. Rev. B **94**, 140414(R) (2016).

[40] A. Ghosh, S. Auffret, U. Ebels, and W. E. Bailey, Penetration depth of transverse spin current in ultrathin ferromagnets, Phys. Rev. Lett. **109**, 127202 (2012).

[41] M. S. Gabor, T. Petrisor, R. B. Mos, M. Nasui, C. Tiusan, and T. Petrisor, Interlayer exchange coupling in perpendicularly magnetized Pt/Co/Ir/Co/Pt structures, J. Phys. D: Appl. Phys. **50**, 465004 (2017).

[42] D. Ourdani, Y. Roussigné, S. M. Chérif, M. S. Gabor, and M. Belmeguenai, Correlation between interface perpendicular magnetic anisotropy and interfacial Dzyaloshinskii–Moriya interactions in Pt/Pd(t_{Pd})/Co(t_{Co})/Au, J. Phys. D: Appl. Phys. **55**, 485004 (2022).

[43] N. Nakajima, T. Koide, T. Shidara, H. Miyauchi, H. Fukutani, A. Fujimori, K. Iio, T. Katayama, M. Nývlt, and Y. Suzuki, Perpendicular magnetic anisotropy caused by interfacial hybridization via enhanced orbital moment in Co/Pt multilayers: Magnetic circular x-ray dichroism study, Phys. Rev. Lett. **81**, 5229 (1998).

[44] Y. Liu, Z. Yuan, R. J. H. Wesselink, A. A. Starikov, and P. J. Kelly, Interface enhancement of gilbert damping from first principles, Phys. Rev. Lett. **113**, 207202 (2014).

[45] K. Gupta, R. J. H. Wesselink, R. Liu, Z. Yuan, and P. J. Kelly, Disorder dependence of interface spin memory loss, Phys. Rev. Lett. **124**, 087702 (2020).

[46] V. P. Amin and M. D. Stiles, Spin transport at interfaces with spin-orbit coupling: Formalism, Phys. Rev. B **94**, 104419 (2016).

[47] W. Zhang, W. Han, X. Jiang, S.-H. Yang, and S. S. P. Parkin, Role of transparency of platinum–ferromagnet interfaces in determining the intrinsic magnitude of the spin Hall effect, Nat. Phys. **11**, 496 (2015).

[48] A. Kalitsov, S. A. Nikolaev, J. Velev, M. Chshiev, and O. Mryasov, Intrinsic spin-orbit torque in a single-domain nanomagnet, Phys. Rev. B **96**, 214430 (2017).

[49] K.-S. Ryu, S.-H. Yang, L. Thomas, and S. S. P. Parkin, Chiral spin torque arising from proximity-induced magnetization, Nat. Commun. **5**, 3910 (2014).

[50] T. A. Peterson, A. P. McFadden, C. J. Palmstrøm, and P. A. Crowell, Influence of the magnetic proximity effect on spin-orbit torque efficiencies in ferromagnet/platinum bilayers, Phys. Rev. B **97**, 020403(R) (2018).

[51] A. Manchon, C. Ducruet, L. Lombard, S. Auffret, B. Rodmacq, B. Dieny, S. Pizzini, J. Vogel, V. Uhlíř, M. Hochstrasser, and G. Panaccione, Analysis of oxygen induced anisotropy crossover in Pt/Co/MO_x trilayers, J. Appl. Phys. **104**, 043914 (2008).

[52] H. X. Yang, M. Chshiev, B. Dieny, J. H. Lee, A. Manchon, and K. H. Shin, First-principles investigation of the very large perpendicular magnetic anisotropy at Fe|MgO and Co|MgO interfaces, Phys. Rev. B **84**, 054401 (2011).

[53] Y. Yang, J. Yuan, L. Qi, Y. Wang, Y. Xu, X. Wang, Y. Feng, B. Xu, L. Shen, and Y. Wu, Unveiling the role of Co-O-Mg bond in magnetic anisotropy of Pt/Co/MgO using atomically controlled deposition and in situ electrical measurement, Phys. Rev. B **95**, 094417 (2017).

[54] M. Belmeguenai, Y. Roussigné, S. M. Chérif, A. Stashkevich, T. Petrisor, M. Nasui, and M. S. Gabor, Influence of the capping layer material on the interfacial Dzyaloshinskii–Moriya interaction in Pt/Co/capping layer structures probed by Brillouin light scattering, J. Phys. D: Appl. Phys. **52**, 125002 (2019).

[55] M. Belmeguenai, J.-P. Adam, Y. Roussigné, S. Eimer, T. Devolder, J.-V. Kim, S. M. Cherif, A. Stashkevich, and A. Thiaville, Interfacial Dzyaloshinskii-Moriya interaction in perpendicularly magnetized Pt/Co/AlOx ultrathin films measured by Brillouin light spectroscopy, Phys. Rev. B **91**, 180405(R) (2015).

[56] S. Bandiera, R. C. Sousa, B. Rodmacq, and B. Dieny, Asymmetric interfacial perpendicular magnetic anisotropy in Pt/Co/Pt trilayers, IEEE Magn. Lett. **2**, 3000504 (2011).

[57] D. Ourdani, Y. Roussigné, S. M. Chérif, M. S. Gabor, and M. Belmeguenai, Dependence of the interfacial Dzyaloshinskii-Moriya interaction, perpendicular magnetic anisotropy, and damping in Co-based systems on the thickness of Pt and Ir layers, Phys. Rev. B **104**, 104421 (2021).

[58] X. Wang and A. Manchon, Diffusive spin dynamics in ferromagnetic thin films with a Rashba interaction, Phys. Rev. Lett. **108**, 117201 (2012).

[59] K. Fuchs, The conductivity of thin metallic films according to the electron theory of metals, Math. Proc. Cambridge Philos. Soc. **34**, 100 (2008).

[60] E. H. Sondheimer, The mean free path of electrons in metals, Adv. Phys. **1**, 1 (1952).

[61] Z. B. Guo, W. B. Mi, R. O. Aboljadayel, B. Zhang, Q. Zhang, P. G. Barba, A. Manchon, and X. X. Zhang, Anomalous Nernst and Hall effects in magnetized platinum and palladium, Phys. Rev. B **86**, 104433 (2012).

[62] P. Zhang, W. Lin, D. Wu, Z. Jiang, and H. Sang, Effective anomalous Hall coefficient in an ultrathin Co layer sandwiched by Pt layers, J. Appl. Phys. **115**, 063908 (2014).

[63] C. L. Canedy, X. W. Li, and G. Xiao, Large magnetic moment enhancement and extraordinary Hall effect in Co/Pt superlattices, Phys. Rev. B **62**, 508 (2000).

[64] F. J. A. den Broeder, W. Hoving, and P. J. H. Bloemen, Magnetic anisotropy of multilayers, J. Magn. Magn. Mater. **93**, 562 (1991).